polymers

MDPI

Article

FDM 3D Printing and Properties of PBS/PLA Blends

Wangwang Yu [1,†], Liwei Sun [2,†], Mengya Li [2], Meihui Li [2], Wen Lei [2,*] and Chaohui Wei [2]

[1] School of Mechanical Engineering, Nanjing Vocational University of Industry Technology, Nanjing 210023, China
[2] College of Science, Nanjing Forestry University, Nanjing 210037, China
* Correspondence: leiwen@njfu.edu.cn; Tel.: +86-25-8542-7621
† These authors contributed equally to this work.

Abstract: Poly(lactic acid) (PLA) and Poly(butylene succinate) (PBS) were chosen as raw materials and melt blended by a twin screw extruder and pelletized; then, the pellets were extruded into filaments; after that, various PBS/PLA blending samples were prepared by Fused Deposition Molding (FDM) 3D printing technology using the filaments obtained and the effect of the dosage of PBS on technological properties of 3D-printed specimens was investigated. For comparison, the PLA specimen was also prepared by FDM printing. The tensile strength, tensile modulus, thermal stability, and hydrophilicity became poorer with increasing the dosage of PBS, while the flexural strength, flexural modulus, impact strength, and crystallinity increased first and then decreased. The blend containing 10% PBS (10% PBS/PLA) had the greatest flexural strength of 60.12 MPa, tensile modulus of 2360.04 MPa, impact strength of 89.39 kJ/m^2, and crystallinity of 7.4%, which were increased by 54.65%, 61.04%, 14.78%, and 51.02% compared to those of printed PLA, respectively; this blend also absorbed the least water than any other specimen when immersed in water. Different from the transparent PLA filament, 10% PBS/PLA filament presented a milky white appearance. The printed 10% PBS/PLA specimen had a smooth surface, while the surface of the printed PLA was rough. All the results indicated that the printed 10% PBS/PLA specimen had good comprehensive properties, including improved mechanical properties, crystallization performance, and surface quality than PLA, as well as proper wettability and water absorption. The prominent conclusion achieved in this work was that 10% PBS/PLA should be an ideal candidate for biodegradable feedstock among all the PBS/PLA blends for FDM 3D printing.

Keywords: poly(lactic acid); poly(butylene succinate); blend; fused deposition molding; 3D printing; property

check for updates

Citation: Yu, W.; Sun, L.; Li, M.; Li, M.; Lei, W.; Wei, C. FDM 3D Printing and Properties of PBS/PLA Blends. *Polymers* **2023**, *15*, 4305. https://doi.org/10.3390/polym15214305

Academic Editor: Babak Eslami

Received: 22 September 2023
Revised: 20 October 2023
Accepted: 31 October 2023
Published: 2 November 2023

Copyright: © 2023 by the authors. Licensee MDPI, Basel, Switzerland. This article is an open access article distributed under the terms and conditions of the Creative Commons Attribution (CC BY) license (https://creativecommons.org/licenses/by/4.0/).

1. Introduction

3D printing is an emerging manufacturing technology covering a process of manufacturing physical items based on digital 3D model data; this process makes it possible to produce some products with innovative designs and a combination of materials that could not be realized by any other processes [1]. This technique has been used in many areas, including agriculture, civil engineering, packaging, architecture, building, healthcare, biomedical, aviation industry, transportation, and foodstuff [2,3].

As one of the most common 3D printing technologies that can be used to make both daily supplies and industrial products, fused deposition modeling (FDM) has attracted engineers and scientists greatly in recent years because of its wide range, non-toxicity of materials, convenient operation, high production efficiency, little maintenance needed, simple structure of equipment, powerfulness to provide durable printing procedures, simple operation, high strength and toughness of materials [4,5]. It can be performed on a wide range of thermoplastic polymers or composites to allow a filament to be extruded through a small nozzle and build up an object in a melted/softened state on a predefined route layer-by-layer [6]. The polymers or their composites concerned currently

include poly(lactic acid) (PLA) [7,8], polybutylene adipate terephthalate [9,10], poly(vinyl chloride) (PVC) [11], thermoplastic polyurethane elastomer [12], polypropylene [13,14], nylon [15,16], polyetheretherketone [17], polycaprolactone (PCL) [18,19], polyhydroxybutyrate [20], polyamide [6,21], acrylonitrile butadiene styrene (ABS) [6,22], and polyphenylene sulfone [4]. PLA is the best choice for FDM 3D printing owing to its low melting point, excellent mechanical properties, thermal stability, biodegradability, non-toxicity, slight shrinkage during processing, good adhesion to the platform, and good dimensional stability of the printed specimens. Besides these, the market for PLA is thought to be one of the two biopolymers expected to grow the most remarkably [6,7,23].

However, PLA by itself has shortcomings; it is relatively hard, its toughness, flexibility, and elasticity are not so good, its printed specimens are easy to be broken, and it also has poor appearance quality. All these limit the widespread application of PLA in the 3D printing area. It is thus of great significance to modify PLA to improve its weak points and meet the requirement for 3D printing; one of the primary methods is by blending PLA with other polymers [24].

As a typical biopolymer, PBS not only has good mechanical properties but also can be processed conveniently [25] and degrades completely. Blending PBS with PLA can increase the ductility of PLA without loss of biodegradability [26,27]. Thus, PBS was often applied to modify PLA when the PLA products were produced by some traditional processes, such as extrusion, injection molding, and compression molding. For example, Sakaowduen et al. [28] developed PBS/PLA blends by extrusion and compression molding and evaluated the mechanical performances of five different PBS/PLA (*w*/*w*) blends and compared them with those of PLA. The impact strength of each blend was greater than that of the PLA when highly flexible PBS was blended with PLA. However, the tensile performances became poorer. Suparanon et al. [26] prepared flame-retardant PBS/PLA blends by a compression molding process and experimented with the effects of flame-retardant agents, dosage of PBS, and combination of the two on the physico-mechanical properties of the blends. They found that the impact toughness of the blends containing 20 wt% PBS rose to about 244% that of the PLA, and an increased content of PBS would lead to a significantly improved elongation at break, impact toughness, and the thermal stability of PLA. Saowaroj Chuayjuljit et al. [29] melt blended PBS and PLA using a 20 mm corotating twin-screw extruder; the extrudates were pelletized and then hot compressed into plates. The impact strength, elongation at break, degree of crystallinity, and thermal stability of PBS/PLA blends were all greater than those of the PLA, and the increment in these properties was dependent on the dosages of PBS, but the tensile strength, tensile modulus, and bending strength all were reduced when more PBS was introduced.

Considering that the PBS/PLA products have much better toughness than that of pure PLA by the traditional processes, in order to solve the drawbacks of neat PLA as the printing material and get the samples with high appearance quality, in this article, the blend was introduced as filaments for FDM 3D printing technology, deep properties, and structural characterization were done on the samples containing various contents of PBS to ensure that the blends could serve as an ideal feedstock for FDM 3D printing.

2. Experimental

2.1. Materials

PLA pellet(3052D, American Nature Works Co., Minnetonka, MN, USA) was obtained from Suzhou Benfuzhong Plastic Import and Export Co., Ltd., China (Suzhou, China); PBS, TH803S, was obtained from Xinjiang Blue Ridge Tunhe Sci. & Tech. Co., Ltd. (Changji City, Xinjiang, China).

2.2. Sample Preparation

PLA and PBS were oven-dried at 60 °C to constant masses to release the adsorbed water. Then, they were melt blended by the proportions as shown in Table 1 using a twin-screw extruder (SHJ-20, Nanjing Giant Machinery Co., Ltd., Nanjing, China) in the

temperature range between 165 °C and 180 °C. The rotating speed of the screw was 20 rpm, and the extrudates were pelletized and put into a single screw extruder (KS-HXY, HUANXINYANG Electrical Equipment Co., Ltd., Suzhou, China) to prepare the mixed filament whose diameter was controlled within 1.75 ± 0.05 mm.

Table 1. Compositions of different blends.

Sample Codes	PLA	5% PBS/PLA	10% PBS/PLA	15% PBS/PLA	20% PBS/PLA	25% PBS/PLA	30% PBS/PLA
PLA/wt%	100	95	90	85	80	75	70
PBS/wt%	0	5	10	15	20	25	30

The prototypes of the printed specimens were built in CAD software(Auto CAD 2020 Simplified Chinese) and exported as an STL file. The STL file was further sliced into a data file by layers, which was made of Gcode. The STL file was transferred to the printer (MOSHU S108; Hangzhou SHINING 3D Technology Co., Ltd., Hangzhou, China) to make the samples.

We once systematically investigated the effect of printing parameters on the properties of FDM 3D-printed composites and got the optimal printing conditions, as shown in Table 2. Thus, these parameters were adopted in this study to print the samples. Printing was carried out in a standard laboratory without temperature or humidity control.

Table 2. Printing parameters of different blends [30].

Parameter	Nozzle Temperature/°C	Platform Temperature/°C	Printing Speed/ mm/s	Layer Thickness/ mm
value	220	50	50	0.1

2.3. Testing and Characterization

2.3.1. Mechanical Testing

The mechanical performances were tested in air at room temperature, among which the tensile test was done referring to ASTM D 638-2010 at a cross-head speed of 10 mm/min, and the bending test was done referring to ASTM D 790-2010 at a cross-head speed of 5 mm/min on a universal mechanical testing machine (E44.304, MTS Industrial Systems (China) Co., Ltd., Shenzhen, China) with a 20 kN load capacity. The impact test was done referring to Chinese National Standard GB/T 1043.1-2008 [31] with a pendulum electronic impact testing machine (XJC-25D, Chengde Precision Testing Machine Co., Ltd., Chengde, China).

2.3.2. Morphological Characterization

The morphology of the surface or the fractured surface of the printed item was observed by using a field-emission scanning electron microscope (SEM) (Hitachi SU 8010, Hitachi Corporation, Tokyo, Japan) at an accelerating voltage of 3 kV. For a better resolution, the surface of each sample was coated with gold before the SEM observation.

2.3.3. Thermal Stability Assessment

TGA was realized by employing a thermo-gravimetric analyzer (NETZSCH-Gerätebau GmbH, Selb, Germany) under a nitrogen atmosphere. The printed specimens (6–8 mg) were heated from 20 °C to 550 °C using a heating rate of 20 °C/ min. The onset temperature at which the sample began to decompose, and the peak temperature at which the specimen decomposed the fastest were investigated to assess the effect of the PBS content on the thermal stability of the printed items.

2.3.4. Melt and Crystallization Behavior

The melt and crystallization behavior test was done in three steps on a differential scanning calorimetry (DSC) instrument (DSC214, NETZSCH-Gerätebau GmbH, Selb, Germany). First, the 5–10 mg sample was heated from room temperature to 220 °C at 15 °C/min under a nitrogen atmosphere and held isothermally for 5 min; then, the specimen was cooled down to room temperature. Finally, the sample was reheated to 220 °C. The transition temperatures and heat capacities were obtained using the NETZSCH analysis software (Proteus70). The crystallinity was calculated using the following equation, considering the polymer fraction in the printed sample:

$$x_c = \frac{|\Delta H_m + \Delta H_{cc}|}{\omega \Delta H^*} \quad (1)$$

where x_c represented the degree of crystallinity of the specimen, ω was the mass content of PLA in the specimen, ΔH_m, ΔH_{cc}, and ΔH^* were the enthalpies of melting, cold crystallization and melting of 100% crystalline PLA, which was found to be 93 J/g in the literature [2,32,33].

2.3.5. Visual Appearance Observation

For comparison, the filaments and the printed samples of neat PLA and 10% PBS/PLA samples were put on a desk with a black background, and then the filaments and the surfaces of the printed items were photographed using a mobile phone with a resolution of twelve million pixels.

2.3.6. Wettability Testing

The contact angle (θ) of distilled water drops on the surface of each FDM 3D-printed specimen was measured at room temperature using a contact angle instrument (DSA100; KRÜSS GmbH, Borsteler Chaussee, Hamburg, Germany). A 5 μL droplet of distilled water was dropped onto the surface and kept for 15 s, and then the θ values were read at various points.

2.3.7. Water Absorption Testing

Water absorption was tested referring to the ASTM D570-98 [34]. The samples were put into a bath containing tap water at room temperature; after 24 h, the samples were taken out from the water, and the water adsorbed onto the surfaces of the samples was removed using an absorbent lint-free cloth; after that, the samples were weighed in a balance whose precision was 0.1 mg. Next, the samples were submerged in water again. The water absorption x_t was obtained using Equation (2), where w_0 and w_t denoted the initial dry mass and the current mass of the samples, respectively. The test was repeated five times, and the averaged values were recorded as the final result.

$$x_t = \frac{w_t - w_0}{w_0} \times 100\% \quad (2)$$

2.3.8. Melting Flow Rate Determination

The melting flow rate (MFR) of the specimens was tested referring to Chinese National Standard GB/T 3682-2000 [35] to clarify the flowability of the specimens. The samples were weighed and added to the melt index meter (XNR-400, Chengde Jinhe Instrument Manufacturing Co., Ltd., Chengde, China). The MFR was measured at 160 °C and 2.16 kgf.

3. Results and Discussion

3.1. Mechanical Performances

The strengths and elongation at the break of the 3D-printed specimens were plotted in Figure 1. It was revealed that the dosage of PBS had a great effect on the tensile, flexural, and impact properties of the 3D-printed PBS/PLA samples.

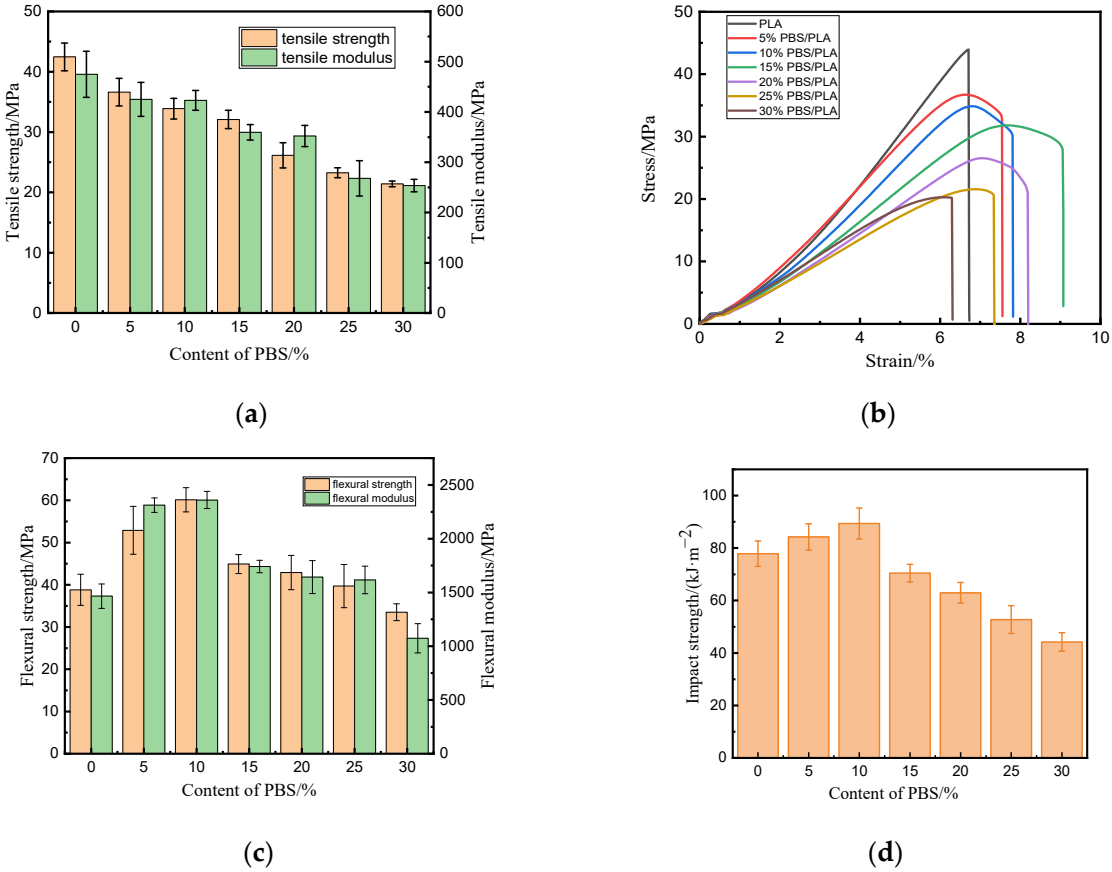

Figure 1. Mechanical performances of PLA and PBS/PLA blends: (**a**) tensile properties; (**b**) σ-ε curves; (**c**) flexural properties; (**d**) impact strength.

The PLA has a relatively brittle behavior with a tensile strength of 42.46 MPa, as illustrated in Figure 1a, which was consistent with the value of 42.27 MPa of the previous study [36]. All the 3D-printed PBS/PLA blends exhibited reduced tensile strength compared to PLA, and the tensile strength decreased monotonically when the PBS content increased; a similar changing trend was once concluded by Justyna et al. [37]; this should be caused by the poor interfacial bonding between PLA and PBS, and also by the low stiffness and ductility of PBS. A similar conclusion could be drawn for the tensile modulus. According to stress–strain curves, with the addition of PBS to PLA, the elastic modulus decreased, indicating that the polymer was softened by PBS. When the content of PBS in the blend was 30%, the tensile strength and modulus of the specimens decreased to 21.41 MPa by 49.58% and 253.66 MPa by 46.58% from those of pure PLA, respectively. The stress–strain curves shown in Figure 1b indicated that pure PLA broke in a brittle manner, while the stress (σ) vs. strain (ε) curve of each PBS/PLA blend could be divided into two parts: a quasi-linear section was observed at first which corresponded to the PBS/PLA interface debonding. Then, a reduction of stress combined with an increasing strain revealed a quasi-ductile behavior; a yield point appeared in each curve of the blends. Furthermore, a greater content of PBS made the blend have a lower yield strength. The enhanced toughness might be because the PBS was a flexible filler and a softer material [26]. It was worth mentioning that the fracture mode of PLA had been changed when PBS was introduced, but no obvious alternation happened to the elongation at the break of the specimen.

For the bending and impact properties, the highest values were all found in the 10% PBS/PLA specimen, followed by the 5% PBS/PLA specimen, meaning that the 10% PBS/PLA blend exhibited the best toughening effect compared to neat PLA, which was a pure polymer. The flexural strength, flexural modulus, and the impact strength of the 10% PBS/PLA blend were 60.12 MPa, 2360.04 MPa, and 89.39 kJ/m^2; a 54.65%, 61.04%,

and 14.78% increase from those of neat PLA, respectively, while they were only 33.50 MPa, 1074.35 MPa, and 44.20 kJ/m^2 for 30% PBS/PLA specimens.

The changing trend of flexural properties was a little different from that of the tensile properties; this might be attributed to the different fracture mechanisms between them. When it was fractured during the flexural test, the sample was actually damaged by compression, shear, and tension simultaneously [38]. Regarding the impact strength, when few PBS was incorporated, it would act as the center of built-in stress and absorb some energy when the sample was affected by an impact force. Thus, the impact strength would increase. When more PBS was introduced, however, the defects arose from the poor interfacial bonding between PBS and PLA, which would reduce the impact strength. As a result, the impact strength first rose and then dropped gradually with the increasing dosage of PBS.

3.2. Morphology

Figure 2 shows the microscopic morphologies of the fracture surfaces of PLA and PBS/PLA blends. The fracture surface of the original PLA was smooth and flat, as observed in the SEM images (Figure 2a), indicating that PLA broke in a brittle manner; this type of fracture manner had previously been reported by some literature [39,40]. After blending with PBS, the microscopic morphologies of the samples containing 5–30% PBS are shown in Figure 2b–g, which are a little rougher than that of neat PLA; in these situations, the blends broke in a ductile manner. This was also in accordance with results from the stress–strain testing, proving that the relative dosage of PBS to PLA affected the mesostructural quality of the obtained products directly. Similar to that of the 3D-printed PCL/PVC blend [41], when PBS content was lower (5% and 10%), the PBS/PLA compounds were single-phase and confirmed that the high molecular affinity of PBS and PLA caused the formation of two miscible compounds. In these two blends, PLA should act as a continuous phase and PBS as the disperse phase, with PBS well dispersed in PLA. However, when more PBS was adopted, partial immiscibility and some defects, such as cleavage and severe plastic deformation, could be observed in the blends, and these defects became more serious when more PBS was applied. The mechanical performances of the specimens were accordingly affected greatly, and the tensile strength of the specimen was thus decreased.

3.3. Thermal Stability

Thermal stability was a critical parameter in the performance evaluation of 3D printing materials [42]. The thermal stability of PLA and PBS/PLA blends was investigated using a hermos-gravimetric analyzer. Figure 3 shows the TGA thermograms and the derivative weight loss in TGA thermograms of samples. All the samples decomposed mainly ranging from 250 to 550 °C; the onset temperature (T_i), the peak temperature at which the sample decomposed fastest (T_p), and the char residue after decomposition are summarized in Table 3.

PLA began to decompose at 351.8 °C, which was faster between 360–400 °C, and the T_p was 377.7 °C. The PBS/PLA blends showed similar trends in thermal degradation with increasing temperature. The thermal degradation of these blends started at lower initial temperatures of thermal degradation and continued to 390–420 °C; this might be due to the lower T_i value of PBS (300 °C) [43] than that of PLA. In the DTG curves, PLA, 5%PBS/PLA, 10%PBS/PLA, or 15% PBS/PLA all had one peak between 350–450 °C. However, the 20%PBS/PLA, 25%PBS/PLA, and 30%PBS/PLA all exhibited two peaks; the temperatures corresponding to the main peaks were 370.1 °C, 369.4 °C, and 365.5 °C, respectively; meanwhile, a shoulder peak around 408 °C could be observed on the right of the main peak for these three specimens, the main and shoulder peaks might correspond to the thermal decomposition of PLA and PBS. Furthermore, the shoulder peak became more visible with the increasing dosage of PBS in the blend, indicating that the phase separation between the two polymers became more serious. These results demonstrated that blending with PBS had a negative effect on the thermal stability of PLA, and the samples became

more unstable when the PBS content was increased; blending a small amount of PBS with PLA, the two polymers were miscible when more PBS was used. However, the interfacial compatibility and cohesion between the two polymers became poorer.

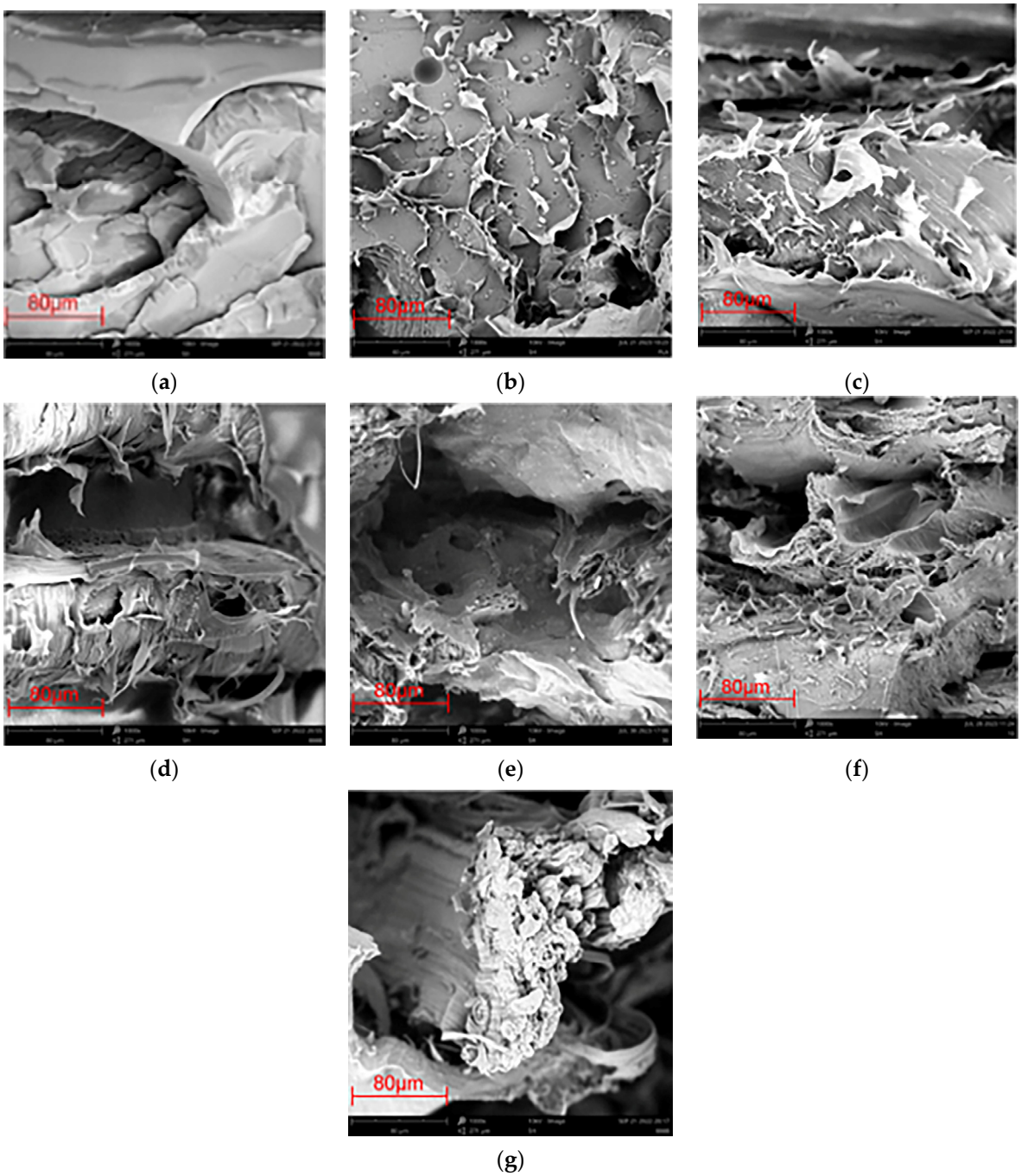

Figure 2. SEM Images of neat PLA and various PBS/PLA blends: (**a**) PLA; (**b**) 5% PBS/PLA; (**c**) 10% PBS/PLA; (**d**) 15% PBS/PLA; (**e**) 20% PBS/PLA; (**f**) 25% PBS/PLA; (**g**) 30% PBS/PLA.

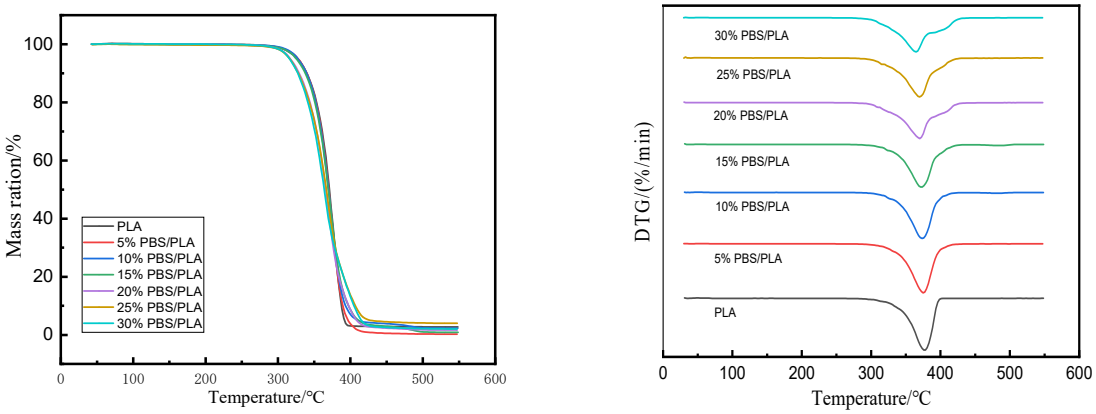

(**a**) (**b**)

Figure 3. Pyrolysis process of PLA and PBS/PLA blends: (**a**) mass loss curve; (**b**) differential thermogravimetric curve.

Table 3. Thermogravimetric analysis data of PLA and 3D-printed PBS/PLA blends.

Sample Code	T_i/°C	$T_{p,1}$/°C	$T_{p,2}$/°C	W/% (550 °C)
PLA	351.8	377.7		2.74
5% PBS/PLA	349.5	375.8		0.25
10% PBS/PLA	347.8	373.9		2.30
15% PBS/PLA	346.0	372.3		0.87
20% PBS/PLA	339.3	370.1	408.33	3.98
25% PBS/PLA	338.5	369.4	407.87	2.27
30% PBS/PLA	333.3	365.5	407.14	2.04

3.4. Melt and Crystallization Behavior

Because of the slow crystallization rate of PLA, the crystallization performance of PLA has attracted much attention [32]. The heating-run curves of the various PBS/PLA blends obtained by the DSC analysis are shown in Figure 4. The total DSC characteristics of the PBS/PLA blends are summarized in Table 3.

It can be found in Figure 4 that all the samples show no melting-crystallization peak during the cooling stage, and a big cold-crystallization peak appeared during the second heating process. The reason could be that it was hard for PLA to organize its molecular chains in a timely manner, and thus, it would crystallize very slowly [32]. The calculated results in Table 4 reveal that the cold-crystallization temperature first rose, then dropped when the dosage of PBS increased. The T_{cc} for neat PLA was 124.2 °C, while that for the 10%PBS/PLA was 128.2 °C, a 4 °C increase from that of PLA, which was also the greatest among all the blends. The higher T_{cc} meant the 10%PBS/PLA started to crystallize earlier than PLA, indicating that a small amount of PBS could promote the crystallization of PLA [27,44]. When more PBS was adopted, the crystallization of PLA might be hindered by PBS because of the aggregation occurring between PBS molecules. This could also be evidenced by the calculated degree of crystallinity in Table 3; the X_c values of the samples rose slightly at first and then reduced with the increase of the mass fraction of PBS in the blend. The 10% PBS/PLA blend had the greatest X_c value of 7.4%.

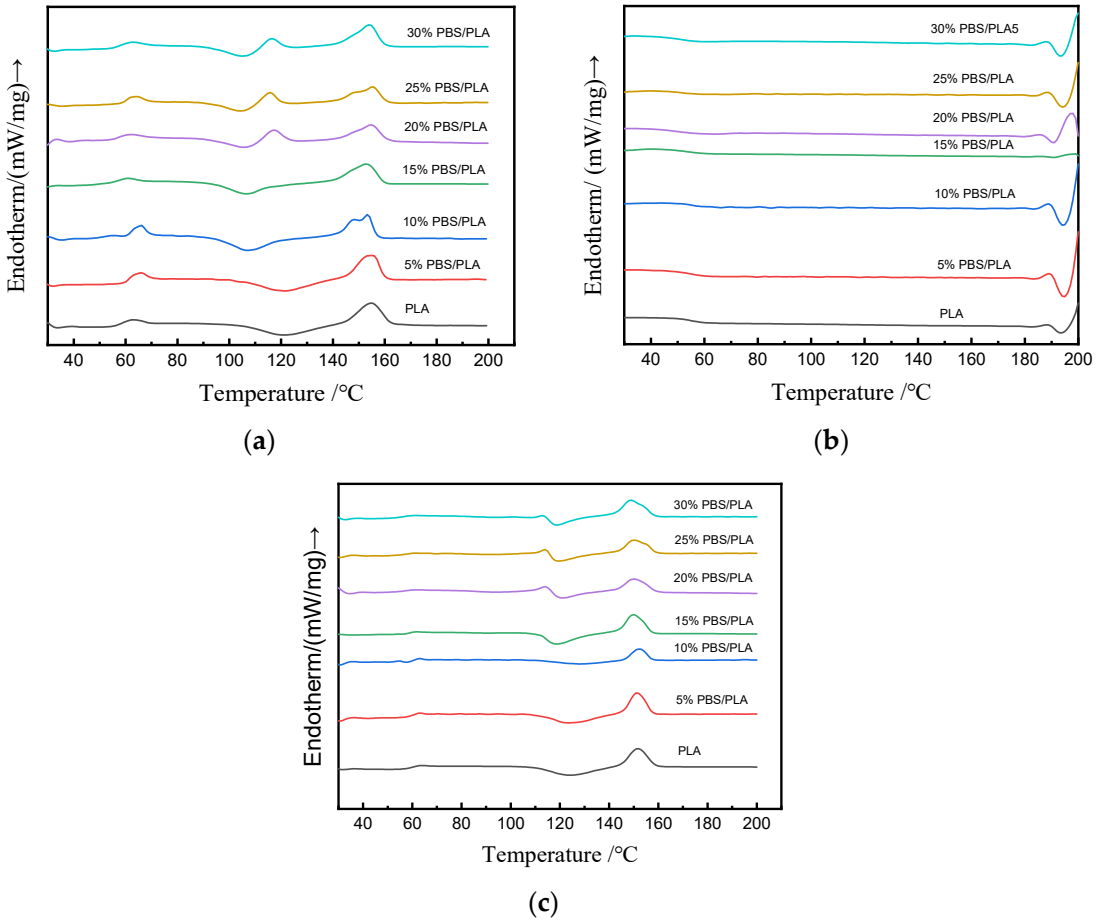

Figure 4. DSC thermograms of printed samples with different contents of PBS: (**a**) first heating, (**b**) cooling, (**c**) second heating.

Table 4. DSC thermal information of different specimens.

Mass Fraction of PBS/wt%	Tg/°C	Tcc/°C	Tm/°C	ΔHcc/(J/g)	ΔHm/(J/g)	Xc/%
0	63.8	124.2	151.7	−18.53	23.17	4.9
5	63.1	124.6	151.4	−18.96	23.74	5.4
10	62.9	128.2	152.3	−5.83	12.3	7.4
15	61.8	121.9	151.7	−11.71	17	6.7
20	61.7	119.8	150.4	−14.59	18.87	5.7
25	61.3	119.8	150.1	−15.8	19.51	5.3
30	61.2	118.7	148.8	−18.77	21.42	4.1

The glass transition temperature (T_g), shown in Table 3, shows that the T_g of neat PLA was 63.8 °C, which was very close to the values of 65.0 °C reported by Marie-Joo et al. [1] and 60.9 °C reported by Yelda et al. [45], and the observation of T_g changing for the blends showed that the glass transition temperatures of PLA would be reduced slightly with the increase of PBS content in the blend. For example, T_g for the blend [PBS/PLA] = [10/90] was 62.9 °C, and for the blend [PBS/PLA] = [20/80], T_g reduced to 61.7 °C, which were 0.9 °C and 2.1 °C lower than that of pure PLA, respectively. The reason was that the content of PBS in the printed samples was relatively low and thus could disperse well in the blend, leading to partial miscibility of the polymers in the amorphous phase [37]; the mobility of the polymer chains was thus less restricted.

3.5. Visual Appearance

The print quality of the samples was affected by many factors, and the two most important factors were the printing parameter [46] and the composition of the blends. We once optimized the printing parameters such as printing speed, printing angle, nozzle temperature, platform temperature, and layer thickness. In this research, the samples were prepared on the optimizing printing conditions, and the emphasis was thus put on the effect of the composition of the blends on the print quality.

As aforementioned, 10% PBS/PLA had the best interfacial bonding between PBS and PLA among all the printed blends; PBS could be fused into PLA the best. Meanwhile, it had improved flexural and impact properties, as well as increased crystallinity than pure PLA. In this part, the visual appearances of PLA and 10% PBS/PLA were comparatively observed, as illustrated in Figure 5.

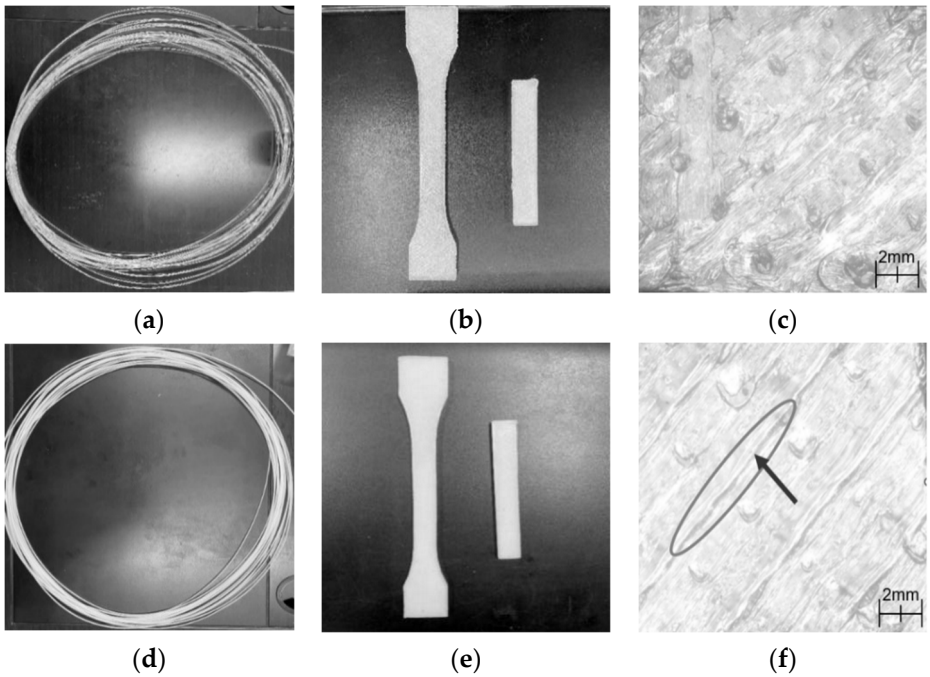

(**a**) (**b**) (**c**)

(**d**) (**e**) (**f**)

Figure 5. Visual appearance of (**a**) PLA filament; (**b**) printed PLA; (**c**) 10% PBS/PLA filament; (**d**) printed 10% PBS/PLA; and surface morphology: (**e**) printed PLA; (**f**) printed 10% PBS/PLA.

Figure 5a,b shows that the PLA filament was transparent, and its printed sample had an uneven surface. However, the 10% PBS/PLA filament was milky white (Figure 5c), and its surface became much smoother (Figure 5d). The SEM observation with a magnification of 40 times indicated that the adjacent filaments in the printed 10% PBS/PLA specimen could bind together tightly (Figure 5f); for the printed PLA specimen, however, many protruding small dots were produced due to the overflow of the PLA melt (Figure 5e). All these indicated that blending the proper amount of PBS with PLA could improve the appearance quality of the printed samples.

3.6. Wettability

The shapes of the water droplets on the surfaces of the specimens are illustrated in Figure 6, and the corresponding contact angles are tabulated in Table 5.

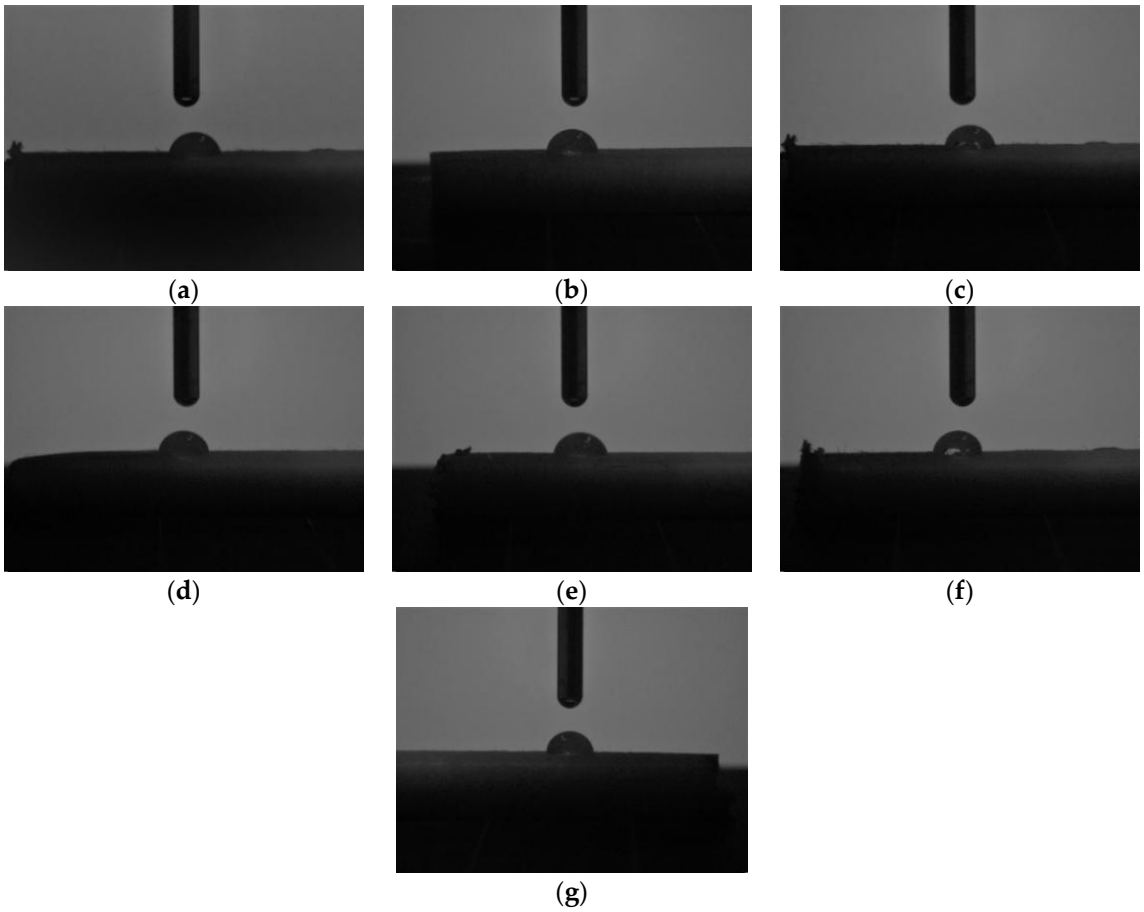

Figure 6. Contact angle images of distilled water on the surfaces of obtained specimens: (**a**) PLA; (**b**) 5% PBS/PLA; (**c**) 10% PBS/PLA; (**d**) 15%PBS/PLA; (**e**) 20% PBS/PLA; (**f**) 25% PBS/PLA; (**g**) 30% PBS/PLA.

Table 5. Contact angles of distilled water on the surfaces of printed samples with different contents of PBS.

Sample	PLA	5% PBS/ PLA	10% PBS/ PLA	15% PBS/PLA	20% PBS/PLA	25% PBS/PLA	30% PBS/ PLA
Contact angle/°	70.8 ± 0.5	74.1 ± 0.4	75.6 ± 0.6	77.2 ± 0.5	78.1 ± 0.4	79.3 ± 0.4	83.4 ± 0.5

It could be noticed that, on the one hand, the water contact angle on the surface of each sample was smaller than 90 °, indicating that the surfaces of all the samples were hydrophilic and could be wetted with water. On the other hand, the surface wettability of the samples varied with the dosage of PBS; the water contact angles for PLA in Figure 6a and Table 4 were 70.8°. After being blended with PBS, the surface contact angle of the blends increased; in addition, the value showed a monotonic increasing trend. The 30% PBS/PLA had a contact angle of 83.4°, which was 12.6° increased remarkably from that of pure PLA, indicating that the hydrophobicity of the specimens was enhanced. The inducement of PBS improved the hydrophobicity of PLA significantly, which might be due to the introduction of a large amount of hydrophobic ester groups in PBS.

During the production of the blends, PBS was assumed to behave as a solid phase and PLA as a liquid phase; when the surface free energy of the fluid was equal to or lower than that of the solid, the two phases would fuse well [47]. The surface free energy was caused by intermolecular interactions at an interface, and it had a relationship with and could be obtained by measuring contact angles [48]. Thus, the increase in the contact angles of the water droplets on the surfaces of the specimens due to the increasing dosage of PBS

could reflect the interfacial compatibilities to some extent; a gradual increase of contact angles meant poorer interfacial compatibility and the mutual fusion between PLA and PBS became more unstable.

3.7. Water Absorption

Figure 7 shows the water uptake of the samples immersed in water for 10 days.

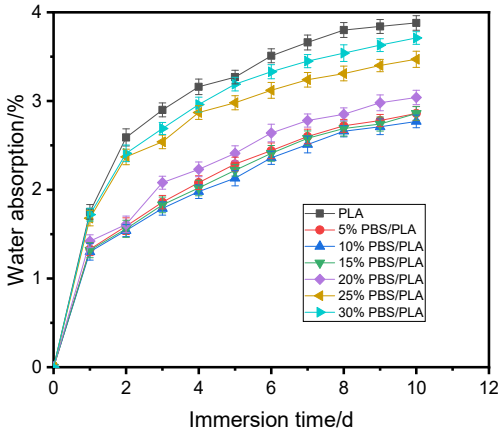

Figure 7. Water absorption curves of different printed samples.

Just like those that happened to many composites [49,50], the rate of water absorption by the printed specimens changed with the immersion time. As observed in Figure 7, the samples absorbed water quickly in the first two days and then gradually slowed down; this changing trend was consistent with the Fickian diffusion curve [49]. After immersion in water for 10 days, the water uptake by each sample almost reached equilibrium. The results revealed in Figure 7 demonstrated that all the blends took less moisture than PLA, and at any immersion stage, the water absorption was reduced first with the increase of the PBS content, then rose gradually; 10% PBS/PLA always absorbed the least water. After ten days, the water uptake values of 10% PBS/PLA was only 2.77%, which was lower by 28.61%, 3.25%, 3.25%, 8.88%, 20.17%, and 25.34% than PLA, and 5% PBS/PLA, 15% PBS/PLA, 20% PBS/PLA, 25% PBS/PLA, and 30% PBS/PLA, respectively.

Many factors would affect the water absorption by the printed samples, such as infill density, the composition of the sample, the relative dosage of different components, and the interfacial compatibility [50]. For the printed blend samples in this study, they were all prepared using the same two polymers by the same method. Thus, the relative dosage of PBS to PLA and the interfacial compatibility were critical for the difference in water absorption. As discussed above, when the content of PBS raised from 0 to 10%, PBS could be dispersed in PLA homogeneously, the interfacial compatibility between the two polymers became better, and the defects induced in the printed samples were reduced. Meanwhile, the crystallinity (x_c) increased, as evidenced in Table 3, and the joint actions by all these factors led to a smaller water uptake by the specimen. When more PBS was used, however, the interfacial compatibility in the blend became poorer, and the number of defects increased. As a result, the water absorption rose.

3.8. Flowability

The MFR was investigated to determine the rheological characteristics of the samples. The results are illustrated in Figure 8. It could be found that the MFR value of the samples increased almost linearly with increasing dosage of PBS in the blends; this changing trend had also been observed by Justyna et al. [37] when they investigated the effects of PBS content on the rheological behavior under different temperatures for the injection molding process. The relationship between the dosage of PBS (X) in the blend and the MFR value (Y) of the printed samples could be expressed by the regression equation

Y = 4.30 + 1.32X (R = 0.9942). The slope of 1.32 meant that the dosage of PBS affected the flowability of the PLA, obviously. It was well known that the poor flowability of the melt would make the products easily have some defects such as deformation, shark skin, and wrinkles, which would worsen the surface quality of the specimens. When the proper amount of PBS was blended with PLA, the MFR of the polymer was increased, and the flow performance was improved, which was helpful for the smooth printing of the samples. As a result, high-quality products would be obtained; a more uniform and smoother surface could theoretically be observed for the samples. If the value of MFR was too great, however, the melt would flow too fast, leading to a weakened melt strength and, accordingly, poorer mechanical properties. In this study, the 10% PBS/PLA blend had an MFR of 15.22 g/10 min, its melt could flow more smoothly, and the printing performance was much better when compared with neat PLA; thus, the visual appearance of printed samples could be improved, as observed in Figure 5. Meanwhile, its MFR was much lower than those containing more PBS and thus owned more excellent mechanical properties than other samples, as illustrated in Figure 1.

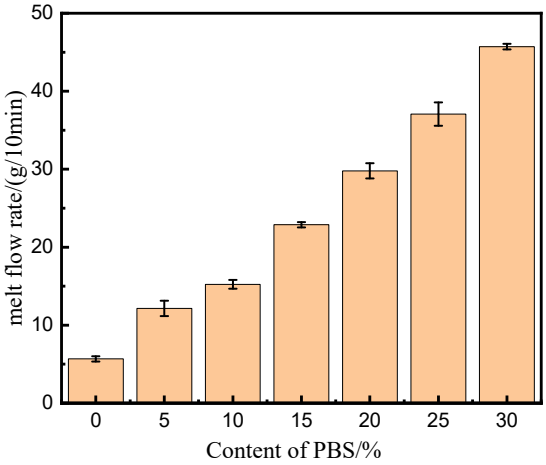

Figure 8. Melt flow rate curves of different samples.

4. Conclusions

In this study, PBS was used to modify PLA for FDM 3D printing, and the mechanical properties, fracture surface morphologies, thermal stability, melt and crystallization behavior, wettability, visual appearance, as well as flowability of various samples were investigated. The concluding remarks of this study are as follows:

1. The tensile properties became poorer when more PBS was used. However, the samples containing 10% PBS had the best bending and impact performances; the bending strength, the flexural modulus, and the impact strength of the printed 10% PBS/PLA sample were 60.12 MPa, 2360.04 MPa, and 89.39 kJ/m^2, which were increased by 54.65%, 61.04%, and 14.78%, respectively, from those of printed PLA samples. After blending with PBS, the fracture of the sample turned from a brittle manner to a little ductile one. SEM observation showed that the fracture surface of the printed PBS/PLA sample became rough while that of the printed PLA sample was smooth. When more PBS was used, serious defects could also be found in the SEM pictures.
2. The printed specimens became more thermally unstable with increasing dosage of PBS. When 10% PBS was used, however, the T_i and T_p were only reduced by 4.0 °C and 3.7 °C, respectively. When 20% or more PBS was used, a shoulder peak appeared on the right of the main peak in each DTG curve.
3. The samples containing 10% PBS had the greatest degree of crystallinity, the least water absorption among all the samples, and a much better visual appearance than pure PLA.

4. With the increasing dosage of PBS, both the water contact angles and the MFR of the samples increased monotonically.

To sum up, blending with the proper amount of PBS contributes to improving the comprehensive printing performance and the quality of the printed samples, among which the best percentage of PBS should be 10%. The excellent comprehensive performances made the 3D-printed PBS/PLA blends have good market prospects in many areas, such as wearable smart devices, bioengineering, and medical devices.

Author Contributions: Conceptualization, W.L. and W.Y.; methodology and formal analysis, W.Y. and W.L.; investigation, L.S., M.L. (Mengya Li), M.L. (Meihui Li) and C.W.; data curation, L.S., W.Y. and W.L.; writing—original draft preparation, W.Y. and L.S.; writing—review and editing, W.L. and W.Y. All authors have read and agreed to the published version of the manuscript.

Funding: This research was funded by The Natural Science Foundation of the Jiangsu Higher Education Institutions of China [22KJA430012].

Institutional Review Board Statement: Not applicable.

Data Availability Statement: The data presented in this study are available on request from the corresponding author.

Conflicts of Interest: The authors declare no conflict of interest.

References

1. Marie-Joo, L.G.; Stefan, H.; Dawn, S.; Beatrix, T.; Evamaria, G.; Abdellatif, B.; Claire, M.L. Influence of rice husk and wood biomass properties on the manufacture of filaments for Fused Deposition Modelling. *Front. Chem.* **2019**, *7*, 735.
2. Agaliotis, E.M.; Ake-Concha, B.D.; May-Pat, A.; Morales-Arias, J.P.; Bernal, C.; Valadez-Gonzalez, A.; Herrera-Franco, P.J.; Proust, G.; Koh-Dzul, J.F.; Carrillo, J.G.; et al. Tensile Behavior of 3D Printed Polylactic Acid (PLA) Based Composites Reinforced with Natural Fiber. *Polymers* **2022**, *14*, 3976. [CrossRef] [PubMed]
3. Shahrubudina, N.; Lee, T.C.; Ramlan, R.; Jen, T.C.; Akinlabi, E.; Olubambi, P.; Augbavboa, C. An Overview on 3D Printing Technology: Technological, Materials, and Applications. *Procedia Manuf.* **2019**, *35*, 1286–1296. [CrossRef]
4. Slonov, A.L.; Khashirov, A.A.; Zhansitov, A.A.; Rzhevskaya, E.V.; Khashirova, S.Y. The influence of the 3D-printing technology on the physical and mechanical properties of polyphenylene sulfone. *Rapid Prototyp. J.* **2018**, *24*, 1124–1130. [CrossRef]
5. Yao, T.Y.; Ye, J.; Deng, Z.C.; Zhang, K.; Ma, Y.B.; Ouyang, H.J. Tensile failure strength and separation angle of FDM 3D printing PLA material: Experimental and theoretical analyses. *Compos. Part B-Eng.* **2020**, *188*, 107894. [CrossRef]
6. Davood, R.; Ismaeil, G.; Majid, B.; Karen, A.; Mostafa, B. 4D printing of PLA-TPU blends: Effect of PLA concentration, loading mode, and programming temperature on the shape memory effect. *J. Mater. Sci.* **2023**, *58*, 7227–7243.
7. Mansingh, B.B.; Binoj, J.S.; Tan, Z.Q.; Eugene, W.W.L.; Amornsakchai, T.; Abu Hassan, S.; Goh, K.L. Comprehensive characterization of raw and treated pineapple leaf fiber/polylactic acid green composites manufactured by 3D printing technique. *Polym. Compos.* **2022**, *43*, 6051–6061. [CrossRef]
8. de Kergariou, C.; Saidani-Scott, H.; Perriman, A.; Scarpa, F.; Le Duigou, A. The influence of the humidity on the mechanical properties of 3D printed continuous flax fibre reinforced poly(lactic acid) composites. *Compos. Part A-Appl. Sci. Manuf.* **2022**, *155*, 106805. [CrossRef]
9. Mayer-Laigle, C.; Foulon, L.; Denoual, C.; Pernes, M.; Rondet, E.; Magueresse, A.; Cécile, B.; Habrant, A.; Bourmaud, A.; Païs, G. Flax shives-PBAT processing into 3D printed fluorescent materials with potential sensor functionalities. *Ind. Crops Prod.* **2021**, *167*, 113482. [CrossRef]
10. Singamneni, S.; Smith, D.; LeGuen, M.J.; Truong, D. Extrusion 3D Printing of Polybutyrate-Adipate-Terephthalate-Polymer Composites in the Pellet Form. *Polymers* **2018**, *10*, 922. [CrossRef]
11. Rahmatabadi, D.; Soltanmohammadi, K.; Aberoumand, M.; Soleyman, E.; Ghasemi, I.; Baniassadi, M.; Abrinia, K.; Bodaghi, M.; Baghani, M. Development of Pure Poly Vinyl Chloride (PVC) with Excellent 3D Printability and Macro- and Micro-Structural Properties. *Macromol. Mater. Eng.* **2022**, *308*, 2200568. [CrossRef]
12. Bi, H.J.; Ren, Z.C.; Guo, R.; Xu, M.; Song, Y.M. Fabrication of flexible wood flour/thermoplastic polyurethane elastomer composites using fused deposition molding. *Ind. Crops Prod.* **2018**, *122*, 76–84. [CrossRef]
13. Long, H.B.; Wu, Z.Q.; Dong, Q.Q.; Shen, Y.T.; Zhou, W.Y.; Luo, Y.; Zhang, C.Q.; Dong, X.M. Mechanical and Thermal Properties of Bamboo Fiber Reinforced Polypropylene/Polylactic Acid Composites for 3D Printing. *Polym. Eng. Sci.* **2019**, *59*, E247–E260. [CrossRef]
14. Morales, M.A.; Atencio Martinez, C.L.; Maranon, A.; Hernandez, C.; Michaud, V.; Porras, A. Development and Characterization of Rice Husk and Recycled Polypropylene Composite Filaments for 3D Printing. *Polymers* **2021**, *13*, 1067. [CrossRef] [PubMed]
15. Rashed, K.; Kafi, A.; Simons, R.; Bateman, S. Fused filament fabrication of nylon 6/66 copolymer: Parametric study comparing full factorial and Taguchi design of experiments. *Rapid Prototyp. J.* **2019**, *28*, 1111–1128. [CrossRef]

16. Moradi, M.; Aminzadeh, A.; Rahmatabadi, D.; Rasouli, S.A. Statistical and Experimental Analysis of Process Parameters of 3D Nylon Printed Parts by Fused Deposition Modeling: Response Surface Modeling and Optimization. *J. Mater. Eng. Perform.* **2021**, *30*, 5441–5454. [CrossRef]
17. Wang, P.; Zou, B.; Ding, S.L.; Li, L.; Huang, C.Z. Effects of FDM-3D printing parameters on mechanical properties and microstructure of CF/PEEK and GF/PEEK. *Chin. J. Aeronaut.* **2020**, *34*, 236–246. [CrossRef]
18. Zhang, P.F.; Arceneaux, D.J.; Khattab, A. Mechanical properties of 3D printed polycaprolactone honeycomb structure. *J. Appl. Polym. Sci.* **2018**, *135*, 46018. [CrossRef]
19. Zhao, Y.Q.; Yang, J.H.; Ding, X.K.; Ding, X.J.; Duan, S.; Xu, F.J. Polycaprolactone/polysaccharide functional composites for low-temperature fused deposition modelling. *Bioact. Mater.* **2020**, *5*, 185–191. [CrossRef]
20. Vaidya, A.A.; Collet, C.; Gaugler, M.; Lloyd-Jones, G. Integrating softwood biorefinery lignin into polyhydroxybutyrate composites and application in 3D printing. *Mater. Today Commun.* **2019**, *19*, 286–296. [CrossRef]
21. Zhang, X.; Fan, W.; Liu, T.X. Fused deposition modeling 3D printing of polyamide-based composites and its applications. *Compos. Commun.* **2020**, *21*, 100413. [CrossRef]
22. Osman, M.A.; Atia, M.R.A. Investigation of ABS-rice straw composite feedstock filament for FDM. *Rapid Prototyp. J.* **2018**, *24*, 1067–1075. [CrossRef]
23. Joseph, T.M.; Kallingal, A.; Suresh, A.M.; Mahapatra, D.K.; Hasanin, M.S.; Haponiuk, J.; Thomas, S. 3D printing of polylactic acid: Recent advances and opportunities. *Int. J. Adv. Manuf. Technol.* **2023**, *125*, 1015–1035. [CrossRef] [PubMed]
24. Davood, R.; Kianoosh, S.; Mostafa, P.; Mohammad, A.; Elyas, S.; Ismaeil, G.; Majid, B.; Karen, A.; Mahdi, B. Shape memory performance assessment of FDM 3D printed PLA-TPU composites by Box-Behnken response surface methodology. *Int. J. Adv. Manuf. Technol.* **2023**, *127*, 935–950.
25. Qu, D.Z.; Wang, L.P.; Sun, S.; Gao, H.W.; Bai, Y.P.; Ding, L.P. Properties of poly(butylene-co-isosorbide succinate) after blown film extrusion. *Green Mater.* **2020**, *8*, 68–78. [CrossRef]
26. Suparanon, T.; Phusunti, N.; Phetwarotai, W. Properties and characteristics of polylactide blends: Synergistic combination of poly(butylene succinate) and flame retardant. *Polym. Adv. Technol.* **2018**, *29*, 785–794. [CrossRef]
27. Deng, Y.; Thomas, N.L. Blending poly(butylene succinate) with poly(lactic acid): Ductility and phase inversion effects. *Eur. Polym. J.* **2015**, *71*, 534–546. [CrossRef]
28. Preampree, S.; Thanyapanich, T.; Boonmahittsud, A.; Intatha, U.; Tawichai, N.; Soykeabkaew, N. Effects of mold sealing and fiber volume fraction on properties of rice straw/unsaturated polyester biocomposites. *ScienceAsia* **2020**, *46*, 85–90. [CrossRef]
29. Chuayjuljit, S.; Wongwaiwattanakul, C.; Chaiwutthinan, P.; Prasassarakich, P. Biodegradable Poly(Lactic Acid)/Poly(Butylene Succinate)/Wood Flour Composites: Physical and Morphological Properties. *Polym. Compos.* **2017**, *38*, 2841–2851. [CrossRef]
30. Yu, W.; Shi, J.; Sun, L.; Lei, W. Effects of printing parameters on properties of FDM 3D printed residue of astragalus/polylactic acid biomass composites. *Molecules* **2022**, *27*, 7373. [CrossRef]
31. *GB/T 1043.1-2008*; Plastics-Determination of Charpy Impact Properties-Part 1: Non-Instrumented Impact Test. General Administration of Quality Supervision, Inspection and Quarantine of the People's Republic of China, Standardization Administration of the People's Republic of China: Beijing, China, 2008.
32. Liu, H.; He, H.; Peng, X.D.; Huang, B.; Li, J.X. Three-dimensional printing of poly(lactic acid) bio-based composites with sugarcane bagasse fiber: Effect of printing orientation on tensile performance. *Polym. Adv. Technol.* **2019**, *30*, 910–922. [CrossRef]
33. Caroline, A.M.; Maurice, N.C. Microcrystalline Cellulose Reinforced Polylactic Acid Biocomposite Filaments for 3D Printing. *Polym. Compos.* **2018**, *39*, 1311–1320.
34. *ASTM D 570-98*; Standard Test Method for Water Absorption of Plastics. American Society for Testing and Materials Information Handling Services: West Conshohocken, PA, USA, 2005.
35. *GB/T 3682-2000*; Determination of the Melt Mass-Flow Rate (MFR) and the Melt Volume-Flow Rate (MVR) of Thermoplastics. General Administration of Quality Supervision, Inspection and Quarantine of the People's Republic of China: Beijing, China, 2000.
36. Narlıoğlu, N. Effect of butyric anhydride modification on properties of wood-polylatictic acid 3D printed composites. *Bioresources* **2022**, *17*, 132–143. [CrossRef]
37. Ostrowska, J.; Sadurski, W.; Paluch, M.; Tynski, P.; Bogusz, J. The effect of poly(butylene succinate) content on the structure and thermal and mechanical properties of its blends with polylactide. *Polym. Int.* **2019**, *68*, 1271–1279. [CrossRef]
38. Dhakal, H.N.; Zhang, Z.Y.; Richard, W.O.W. Effect of water absorption on the mechanical properties of hemp fibre reinforced unsaturated polyester composites. *Compos. Sci. Technol.* **2007**, *67*, 1674–1683. [CrossRef]
39. Vidakis, N.; Petousis, M.; Velidakis, E.; Liebscher, M.; Mechtcherine, V.; Tzounis, L. On the Strain Rate Sensitivity of Fused Filament Fabrication (FFF) Processed PLA, ABS, PETG, PA6,and PP Thermoplastic Polymers. *Polymers* **2020**, *12*, 2924. [CrossRef] [PubMed]
40. Khaliq, J.; Gurrapu, D.R.; Elfakhri, F. Effects of Infill Line Multiplier and Patterns on Mechanical Properties of Lightweight and Resilient Hollow Section Products Manufactured Using Fused Filament Fabrication. *Polymers* **2023**, *15*, 2585. [CrossRef]
41. Davood, R.; Mohammad, A.; Kianoosh, S.; Elyas, S.; Ismaeil, G.; Majid, B.; Karen, A.; Mahdi, B.; Mostafa, B. Toughening PVC with biocompatible PCL softeners for supreme mechanical properties, morphology, shape memory effects, and FFF printability. *Macromol. Mater. Eng.* **2023**, *308*, 2300114.
42. Zhang, Q.; Ma, L.S.; Zhang, X.Y.; Zhang, L.L.; Wang, Z.G. Lignocellulose nanoffber/polylactic acid (LCNF/PLA) composite with internal lignin for enhanced performance as 3D printable filament. *Ind. Crops Prod.* **2022**, *178*, 114590. [CrossRef]

43. Park, C.W.; Youe, W.J.; Han, S.Y.; Park, J.S.; Lee, E.A.; Park, J.Y.; Kwon, G.J.; Kim, S.J.; Lee, S.H. Influence of Lignin and Polymeric Diphenylmethane Diisocyante Addition on the Properties of Poly(butylene succinate)/Wood Flour Composite. *Polymers* **2019**, *11*, 1161. [CrossRef]
44. Dai, X.; Cao, Y.; Shi, X.W.; Wang, X.L. Non-isothermal crystallization kinetics, thermal degradation behavior and mechanical properties of poly(lactic acid)/MOF composites prepared by melt-blending methods. *RSC Adv.* **2016**, *6*, 71461–71471. [CrossRef]
45. Meyva-Zeybek, Y.; Kaynak, C. A comparative study for the behavior of 3D-printed and compression molded PLA/POSS nanocomposites. *J. Appl. Polym. Sci.* **2021**, *138*, e50246. [CrossRef]
46. Sunghan, K.; Korolovych, V.F.; Rachel, L.M.; Vladimir, V.T. 3D-printed polymer packing structures: Uniformity of morphology and mechanical properties via microprocessing Conditions. *J. Appl. Polym. Sci.* **2020**, *137*, e49381.
47. Kong, M.R.; Qin, Z.; Zhang, P.; Xie, G.Q.; Wang, H.; Wang, J.; Guan, F.L.; Yang, W.Z.; Qiu, Z.W. Study on modified poplar wood powder/polylactic acid high toughness green 3D printing composites. *Int. J. Biol. Macromol.* **2023**, *228*, 311–322. [CrossRef]
48. Ramírez-González, P.V.; Arriaga, M.M.A.; Escobar-Barrios, V.A. A rapid method for interfacial tension calculation between rock plug and crude oil based on contact angles, application for EOR. *Pet. Sci. Technol.* **2018**, *36*, 1242–1249. [CrossRef]
49. Faure, F.; Perrot, A.; Pimbert, S.; Lecompte, T. Water absorption measurements on WPCs: Assessment of size and direction dependencies in order to design fast and accurate quality control tests. *Polym. Test.* **2019**, *77*, 105899. [CrossRef]
50. Hamdan, M.H.M.; Siregar, J.P.; Cionita, T.; Jaafar1, J.; Efriyohadi, A.; Junid, R.; Kholil, A. Water absorption behaviour on the mechanical properties of woven hybrid reinforced polyester composites. *Int. J. Adv. Manuf. Technol.* **2019**, *104*, 1075–1086. [CrossRef]

Disclaimer/Publisher's Note: The statements, opinions and data contained in all publications are solely those of the individual author(s) and contributor(s) and not of MDPI and/or the editor(s). MDPI and/or the editor(s) disclaim responsibility for any injury to people or property resulting from any ideas, methods, instructions or products referred to in the content.